Volume 8
Number 34
14 September 2020
Pages 11651–11998

Journal of Materials Chemistry C

Materials for optical, magnetic and electronic devices

rsc.li/materials-c

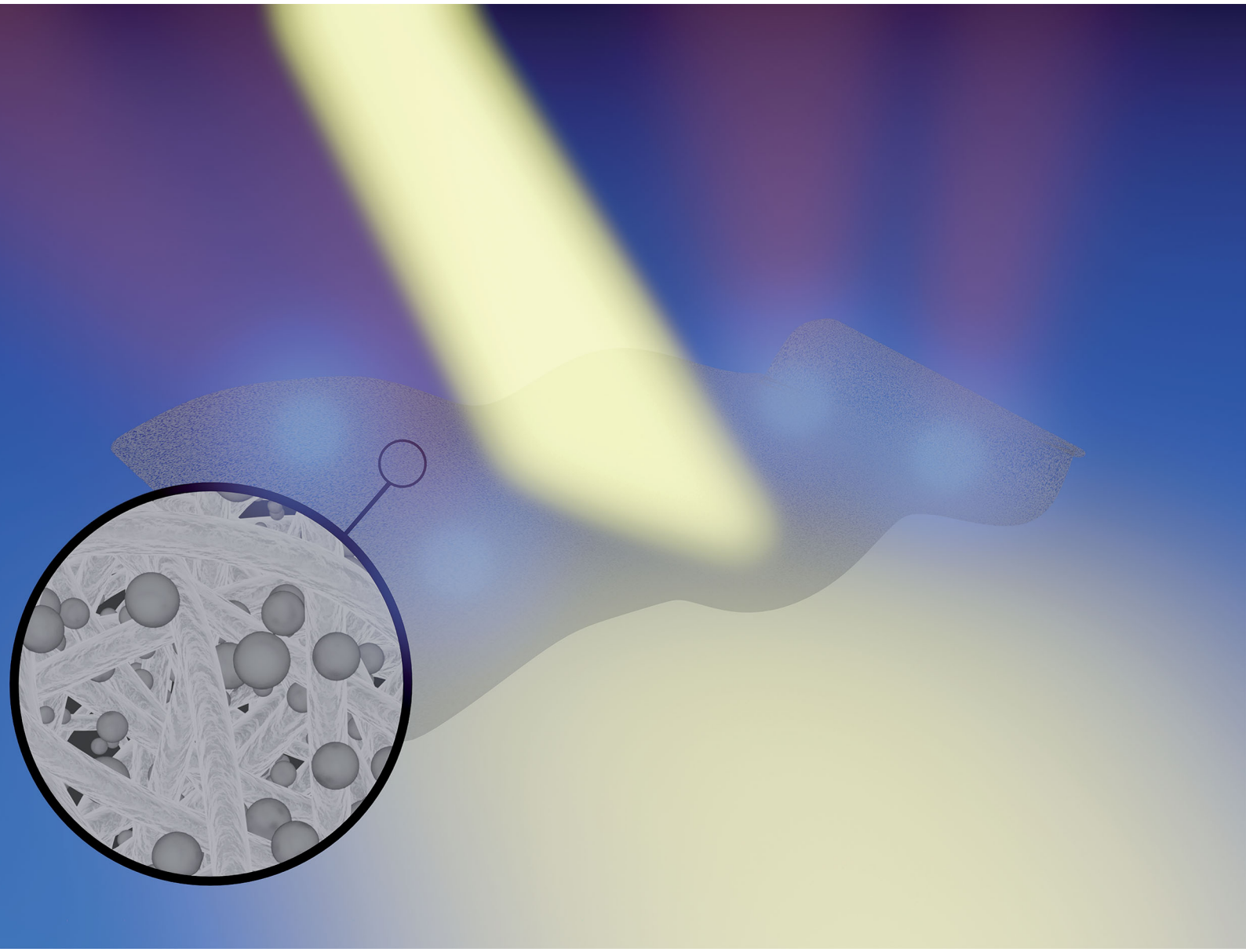

ISSN 2050-7526

ROYAL SOCIETY OF CHEMISTRY

PAPER

Magnus P. Jonsson *et al.*

Transparent nanocellulose metamaterial enables controlled optical diffusion and radiative cooling

Journal of Materials Chemistry C

ROYAL SOCIETY OF CHEMISTRY

PAPER

View Article Online
View Journal | View Issue

Check for updates

Cite this: J. Mater. Chem. C, 2020, 8, 11687

Transparent nanocellulose metamaterial enables controlled optical diffusion and radiative cooling†

Sampath Gamage,[ab] Evan S. H. Kang, ‡[a] Christina Åkerlind,[c] Samim Sardar, §[a] Jesper Edberg,[d] Hans Kariis,[c] Thomas Ederth,[e] Magnus Berggren[ab] and Magnus P. Jonsson *[ab]

Received 9th March 2020,
Accepted 18th June 2020

DOI: 10.1039/d0tc01226b

rsc.li/materials-c

Materials that provide independent control of infrared thermal radiation and haze in the visible could benefit many areas and applications, including clothing, packaging and photovoltaics. Here, we study this possibility for a metamaterial composite paper based on cellulose nanofibrils (CNF) and silicon dioxide (SiO_2) microparticles with infrared (IR) Fröhlich phonon resonances. This CNF–SiO_2 composite shows outstanding transparency in the visible wavelength range, with the option of controlling light diffusion and haze from almost zero to 90% by varying the SiO_2 microparticle concentration. We further show that the transparent metamaterial paper could maintain high thermal emissivity in the atmospheric IR window, as attributed to strong IR absorption of both the nanocellulose and the resonant SiO_2 microparticles. The high IR emissivity and low visible absorption make the paper suitable for passive radiative cooling and we demonstrate cooling of the paper to around 3 °C below ambient air temperature by exposing it to the sky.

1. Introduction

Cellulose is a highly important nontoxic and biodegradable organic material. It has been recognized as an environmentally friendly and sustainable material that can find use in a broad range of applications. In particular, the nanosized version cellulose nanofibrils (CNF) has been in the spotlight owing to its interesting combination of properties, including optical transparency, biocompatibility, low density, and high tensile strength.[1–3] These properties make CNF suitable for various electronic and bioelectronic applications,[1,2] and it has also been explored for optical applications in the areas of electronic displays, structural coloration and many other.[4–13]

The ability to scatter light with minimal absorption losses enables a material to be used as optical diffuser. Optical diffusers play crucial roles in different optical and optoelectronic devices, by improving light uniformity and brightness as well as enhancing device efficiency and sensitivity.[12–21] Motivated by major drawbacks of current diffuser technologies, such as high processing costs and low transmission efficiency, nanocellulose-based systems have been proposed and investigated as promising alternatives.[3,4,12,13]

While transparent in the visible, cellulose instead provides strong absorption in the infrared due to molecular vibrations (*e.g.*, C–O–H bending, C–O stretch, CH_2 wagging, and C=O stretch).[22,23] The corresponding high thermal emissivity makes cellulose-based materials suitable for passive radiative cooling, which so far was only sparsely reported[24] and to our knowledge not previously investigated for nanocellulose composites. In radiative cooling, heat is dissipated to outer space passively *via* emission of thermal radiation in the atmospheric window (8–13 μm). The concept thereby enables sub-ambient cooling of materials without need for external power supply. While radiative cooling systems have generally been based on inorganic thermal photonic structures,[25–29] organic and organic/inorganic hybrid materials are emerging as interesting alternatives, with added benefits such as production scalability and low cost.[24,30–32] It is particularly challenging to achieve a net effect from radiative cooling during daytime, because this requires materials that not only provide high thermal emissivity but also minimal solar-induced heating from absorption in the visible and near-IR spectral ranges.[29,30,33–35] Research on daytime radiative cooling has made significant progress recently, particularly targeting cooling of living spaces to reduce the need for air-conditioning[36,37] and cooling of photovoltaic devices to improve their efficiency and life time.[35,38,39] Other directions include improving cooling performance under extreme conditions[40–42] and creating cooling materials with different colors.[43,44]

[a] Laboratory of Organic Electronics, Department of Science and Technology, Linköping University, SE-601 74 Norrköping, Sweden. E-mail: magnus.jonsson@liu.se
[b] Wallenberg Wood Science Center, Linköping University, SE-601 74 Norrköping, Sweden
[c] FOI-Swedish Defence Research Agency, 583 30 Linköping, Sweden
[d] RISE Acreo, Department of Printed Electronics, Box 787, SE-601 17, Norrköping, Sweden
[e] Division of Biophysics and Bioengineering, IFM, Linköping University, 58183 Linköping, Sweden

† Electronic supplementary information (ESI) available. See DOI: 10.1039/d0tc01226b

‡ Current address: Department of Physics, Chungbuk National University, Cheongju 28644, Republic of Korea.

§ Current address: Center for Nano Science and Technology@PoliMi, Istituto Italiano di Tecnologia, 20133 Milano, Italy.

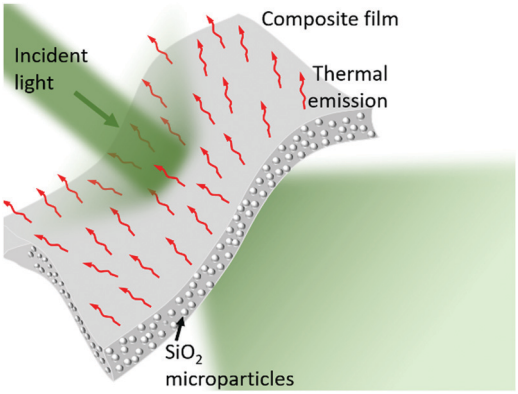

Fig. 1 Schematic illustration depicting the functionality of the composite paper. The shaded green depicts visible light being diffusely transmitted and partly reflected by the paper. The red curvy arrows depict emission of thermal radiation from the surface.

In this work, we address the challenge of simultaneously enabling radiative cooling, high optical transparency, and control of haze. Such combination of properties is of particular interest for photovoltaic and other optoelectronic devices, by providing a passive means of cooling devices[45,46] while simultaneously enhancing their light absorption by acting as optical diffuser.[12,47] The presented material combines nanocellulose and silicon dioxide (SiO_2) microparticles. It is a mechanically flexible and sustainable cellulose-microparticle composite that simultaneously provides controlled optical diffusive properties in the visible spectral range, minimal visible absorption, and strong IR absorption with associated capability for passive radiative cooling. Fig. 1 presents a schematic of the composite paper, illustrating its diffusive and radiative cooling functionalities. Visible light transmits through the paper and is diffusively scattered by the (non-absorbing) SiO_2 microparticles embedded in the material. Simultaneously, the paper emits heat *via* thermal radiation in the atmospheric window due to high emissivity of both the nanocellulose and the microparticles, where the latter provide resonant IR absorption *via* Fröhlich phonon resonances.[48] We used a combination of conventional transmission spectroscopy and integrating sphere spectroscopy to study the influence of microparticle size and concentration on the translucent diffusive properties of the composites. IR integrating sphere measurements further revealed the IR absorptance and, hence thermal emissivity of the composites in the atmospheric IR window, shedding light on their potential use for radiative cooling. Finally, we present demonstrations of passive daylight radiative cooling using the metamaterial composites.

2. Experimental

Sample preparation

Aqueous solutions of 0.52 weight percentage (wt%) carboxymethylated CNF (produced by RISE Bioeconomy) together with commercially available monodispersed, non-porous, amorphous SiO_2 microspheres (Cospheric LLC) of three different diameters, 1.18, 4.3 and 7.75 μm in powder form were used to fabricate samples with final microparticle contents ranging from 0 to ~10 wt%. For all particle sizes used, the coefficient of variance was less than 10%, and more than 95% of the particles were spherical, according to the supplier provided data. For all samples with SiO_2 microparticles, we followed the same fabrication procedure. First, the required weight of microparticle powder for each sample was mixed with water and sonicated to avoid agglomeration. Then the required amount of CNF solution was diluted with water so that the viscosity was low enough to evenly disperse the microparticles. A constant amount of glycerol was added for each sample to decrease stiffness and improve flexibility and smoothness of the samples when dried. The diluted CNF solution with added microparticles and glycerol was sonicated to obtain a homogenous distribution of the microparticles. Next, the resulted mixture was poured into Petri dishes and kept in vacuum to remove any air bubbles, followed by drying in an oven for about 24 h at 60 °C. The CNF films without microparticles were prepared following the same procedure but without adding any microparticles. To study the IR absorption properties of the SiO_2 microparticles, particles of each size were mixed in water, drop-casted and dried on a Si wafer.

Sample characterization

Surface morphology was studied using conventional optical microscopy. For the visible wavelength range, direct transmission spectra were acquired using a 300 W xenon lamp (Newport) and a light guide connected to a spectrograph (Andor Shamrock 303i) with Newton CCD detector. The total (direct and diffuse) transmission was measured by placing the sample in front of the input window of an integrating sphere. For the mid-IR range, the total reflectance R (including backscattering) and transmittance T (including forward scattering) were determined using a Bruker Vertex 70 Fourier Transform IR (FTIR) spectrometer, with an integrating sphere Labsphere A 562 (∅ 75 mm) coated with diffusely reflecting gold. The measurements were performed with a resolution of 16 cm^{-1}. The samples were mounted between two metal sheets with a centered aperture of 20 mm, approximately the same aperture as the aperture of the integrating sphere.

For radiative cooling measurements, five thermocouples were evenly placed in a horizontal plane at the middle of a polyethylene (PE) enclosure of ~40 cm × 40 cm × 40 cm, so that they are equidistant from each other and from the center of the enclosure (see Fig. 5A). Two of the thermocouples were used to measure the ambient temperature in the PE enclosure and the average of these two measurements were plotted as ambient temperature. We connected the three samples to the rest of the thermocouples in such a way that they monitored the temperature of the top surface of each sample, as demonstrated in the schematics in Fig. 5A. All real-time temperature values of thermocouples were recorded using a LabVIEW program interfaced by an Arduino processor.

3. Results and discussion

Fig. 2 shows optical microscopy images of top and bottom surfaces of metamaterial composites with different wt% of

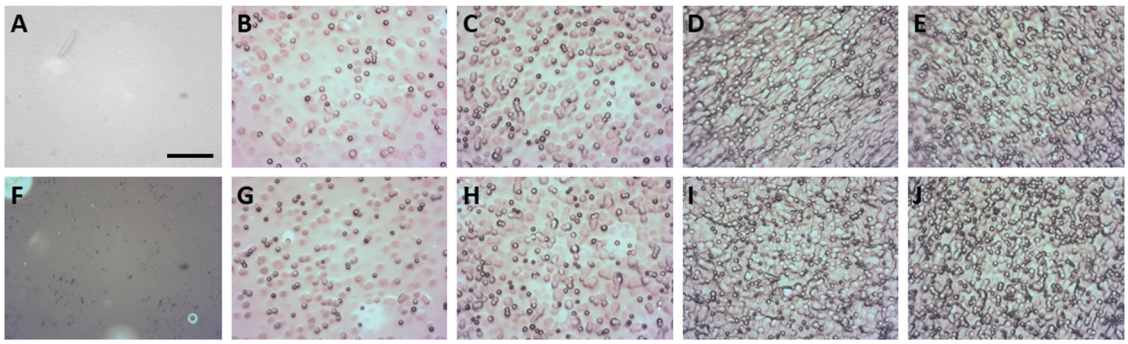

Fig. 2 Optical microscope images of top (top row, A–E) and bottom (bottom row, F–J) sides of CNF/SiO_2 microparticle composite films with particle contents of 0 (no microparticles), 1.6, 3.5, 6.3 and 10.3 wt% from column 1 to column 5, respectively. Particles used are 4.3 μm. The scale bar is 50 μm.

4.3 μm diameter SiO_2 microparticles. The top (Fig. 2A–E) and bottom (Fig. 2F–J) rows present images of the top and bottom sides of the samples, respectively. Each column from left to right correspond to samples with increasing particle concentration, from 0 wt% at the far left to 10.5 wt% at the rightmost column. The results indicate uniform particle distributions for all concentrations, with particles present throughout the thickness of the papers. For the samples with lower SiO_2 contents, the microparticle concentration appears slightly higher when imaged from the bottom side, which may be due to gravitational effects during the drying process of the samples.

We studied the diffusive optical transmission properties of composite films containing microparticles of different sizes and concentrations. Fig. 3A shows the total transmission (T_t) and the direct transmission (T_d) of visible light for six samples with microparticle content ranging from 0 to 10.3 wt% (particle size = 4.3 μm). Importantly, T_t remains above 90% in the whole visible range for all samples, with no significant reduction in T_t even for samples with particle contents up to 10.3 wt%. This result means that visible light absorption (*e.g.*, by solar illumination) in the composite films is very low, and independent absorption measurements indeed show that it is below 5% (see Fig. S1, ESI†). By contrast, T_d shows strong dependence on microparticle content, with T_d decreasing to around 70% already for 1.6 wt% of microparticles. The direct transmission continues to gradually decrease with increasing microparticle content, reaching around 20% at

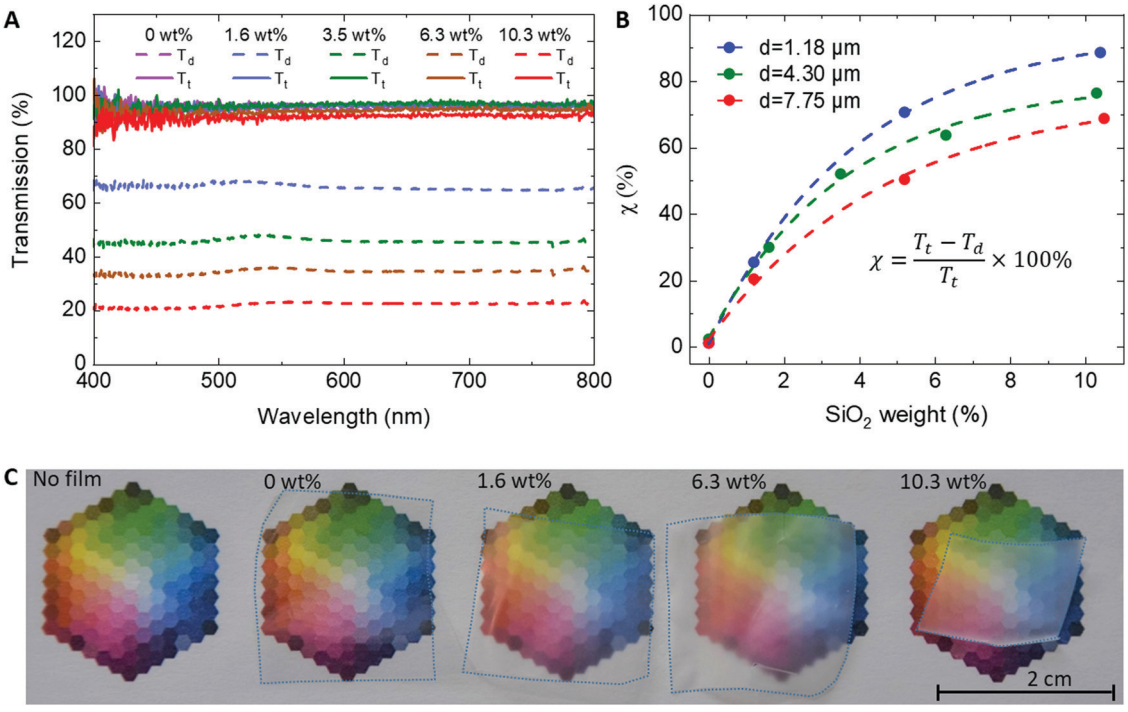

Fig. 3 Dependence of visible transmission on SiO_2 weight% of composite paper. (A) Total (T_t) and direct (T_d) transmission spectra obtained using integrating sphere set up for films with different wt% of 4.3 μm particles. (B) Quantification of scattered transmission fraction (χ) as a function of microparticle wt% for films with three different sizes of particles. The dashed lines act as guides to the eye. (C) Optical images of composite papers with 4.3 μm particles, on top of color pallets to illustrate the effect of particle content on translucency. Film boundaries are marked with grey dashed lines as a guide to the eye.

10.3 wt%. This result is due to increasing number of scatterers in the beam path for films with higher microparticle content, where a gradual increase in thickness may also play a role. Nanocellulose samples without particles of different thicknesses showed no significant variation in neither T_d nor absorption in the relevant thickness range (see Fig. S2, ESI†).

In order to quantify and compare the optical translucent nature of the films, we define the haze parameter, χ as:

$$\chi = \frac{T_t - T_d}{T_t} \times 100\% \quad (1)$$

Fig. 3B shows χ values for three different particle sizes at different concentrations. The blue, green and red dots represent samples with particles of sizes 1.18, 4.3 and 7.75 μm, respectively. The trend is the same for all particle sizes, with χ increasing gradually with increasing particle concentration. This is due to the particles acting as non-absorbing scatterers. Smaller particle size leads to more rapid increase in χ with increasing wt% of microparticles, reaching nearly 90% at 10.3 wt%. We attribute this result to the increase in particle density (number of particles per unit volume) for the same wt% with decreasing particle size. The film with 10.3 wt% of 4.3 μm microparticles showed 75% haze with optical transparency over 90%. These values are highly promising for applying our materials as optical diffusers. As comparison, previous nanocellulose[13] and wood fiber-based[12] materials showed around 60% haze in combination with 90% and 96% optical transparency, respectively.

To visualize the effect of controlling translucency by microparticle content, we took photographs of composite films on top of color palettes printed on a separate paper (Fig. 3C). From left to right we have first a color palette without any sample and then samples with 0, 1.6, 6.3 and 10.3 wt% of microparticles, respectively. There is very little haze seen in the sample without microparticles, for which the color palette below the film looks essentially the same as for the one without any film on top. The haze then increases gradually with increasing microparticle content and it becomes increasingly difficult to see the details of the underlying palette. These results agree with the transmission spectra shown in Fig. 3A and haze parameter presented in Fig. 3B.

After verifying the possibility to control haze, we investigated how the CNF–SiO_2 composite materials behave in the IR spectral range. The intention was to make composites with strong IR absorption and thereby strong thermal emissivity and suitability for passive radiative cooling. The cellulose matrix provides inherent strong IR absorption *via* vibrational resonances and we chose SiO_2 microparticles as visible scatterers as they are known to strongly absorb IR light *via* size-dependent Fröhlich phonon resonances.[30,48,49] Indeed, attenuated total reflection (ATR) IR spectroscopy of microparticles drop-casted onto Si substrates show significant absorption in the relevant wavelength range between 8 μm and 13 μm, as shown in Fig. 4A. The observed differences in the spectral characteristics between microparticles of different diameters (1.18, 4.30 and 7.75 μm) match well with finite-difference time-domain (FDTD) simulations of closely packed SiO_2 microparticles of the same sizes (see Fig. 4B). Both ATR spectra and simulated spectra have been normalized to the peak at around 12.5 μm corresponding to Si–O bending mode, in order to correct for differences due to variations in amount of material for different particle sizes. Simulations of single particles show similar behavior (inset in Fig. 4B), representing particles dispersed in the composite films.

We determined the IR absorptance (*i.e.* emissivity, based on Kirchoff's law of thermal radiation[50,51]) of different composite samples using $1 - T - R$, where R and T are the total transmittance (including forward scattering) and reflectance (including backward scattering), respectively, both obtained using an integrating sphere. Fig. 4C shows the IR absorptance of samples without any particles (black), with 10 wt% microparticles of diameter 7.75 μm (red), and with 10 wt% 1.18 μm in diameter microparticles (purple). All three samples show high absorptance in the atmospheric window. The samples with microparticles show higher IR absorptance than the sample without particles and the sample with smallest microparticles (1.18 μm) provides highest values in this region of interest. While this could be related to highest microparticle density for this sample, we also note that the thicknesses of these three samples were not identical. We therefore further calculated the absorption per unit thickness (absorption coefficient, α) using:[52]

$$\alpha = \frac{1}{t}\ln\left\{\frac{(1-R)^2}{2T} + \sqrt{\left[\frac{(1-R)^2}{2T}\right]^2 + R^2}\right\} \quad (2)$$

where t, R and T are film thickness, total reflectance and total transmittance, respectively. Fig. 4D presents the results, suggesting that part of the differences in absorptance between the samples can be attributed to thickness variations. The sample without microparticles shows somewhat higher α around 9–10 μm while the sample with particles of diameter 1.18 μm provides higher absorption coefficient in most of the remaining broad spectral regions. The main conclusion is that the strong IR absorption of the nanocellulose films is maintained when tuning the visible haze by the addition of the microparticles. The corresponding high IR emissivity makes them promising for radiative cooling applications.

We demonstrate the capability of the metamaterial papers for daytime radiative cooling *via* real-time temperature measurements in Norrköping in Sweden on a day with clear sky and low wind disturbances. Fig. 5 presents the results for a nanocellulose film without microparticles, a sample with 10 wt% microparticles (d = 1.18 μm) and a sample without microparticles but coated with a 150 nm silver (Ag) film on the backside as visible reflector, which may be useful for applications benefiting from preventing visible absorption by materials behind the film. The samples were first connected to thermocouples inside the lab (at ~21 °C) and then the setup was moved outdoor ($T_{ambient}$ ~ 10 °C).

Fig. 5C and D shows the temperature evolution (top panels) of the samples and corresponding temperature difference relative to the ambient temperature (ΔT, bottom panels), for two different time windows. Measurement data for the whole time interval is shown in Fig. S3 (ESI†). Naturally, both the ambient and sample temperatures rapidly decreased once the

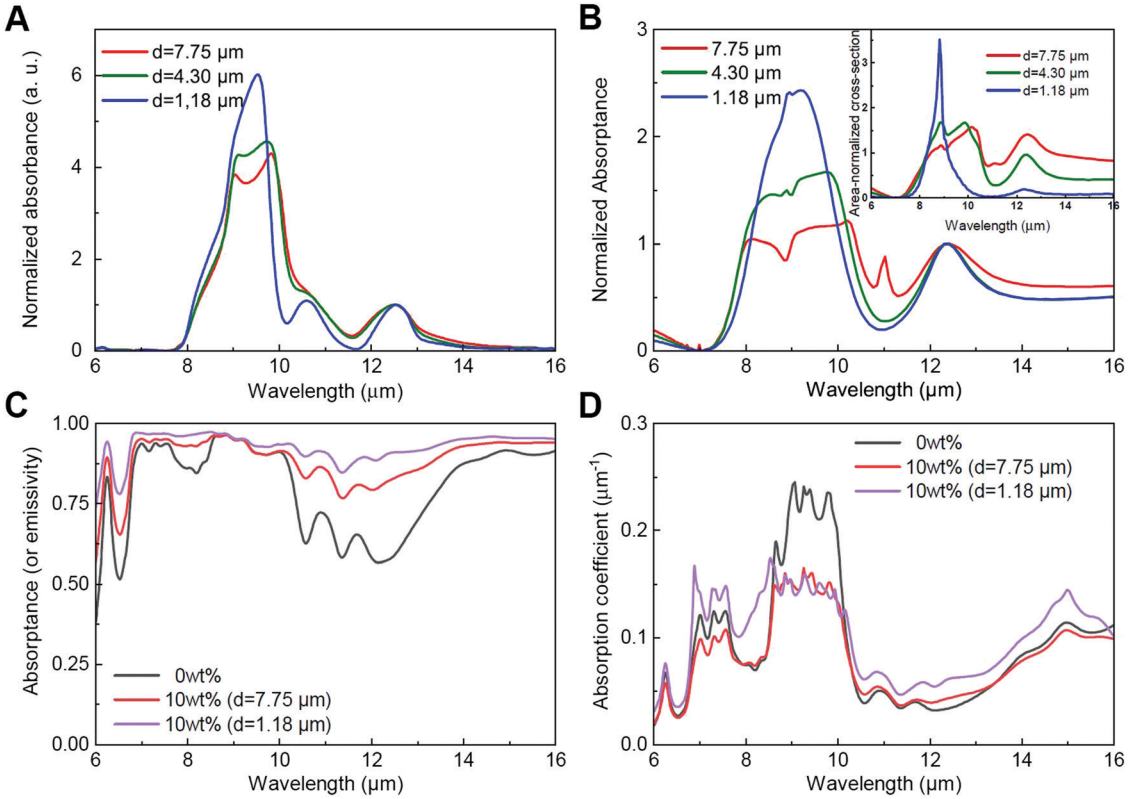

Fig. 4 IR absorption/emission properties of pure SiO_2 particles and metamaterial papers with three different sizes of particles. (A) FTIR-ATR absorbance spectra for SiO_2 particles, normalized to the peak at 12.5 μm. (B) Simulated absorptance for single layers of microparticles that are hexagonally packed, normalized to the peak at 12.5 μm. The inset shows the simulated IR absorption cross-section for single SiO_2 particles. (C) Absorptance (*i.e.* emissivity) and (D) absorption coefficient (α) of composite papers with different microparticle sizes and wt%. The thickness of the film without particles was 31 μm, while the other two samples were around 48 μm thick.

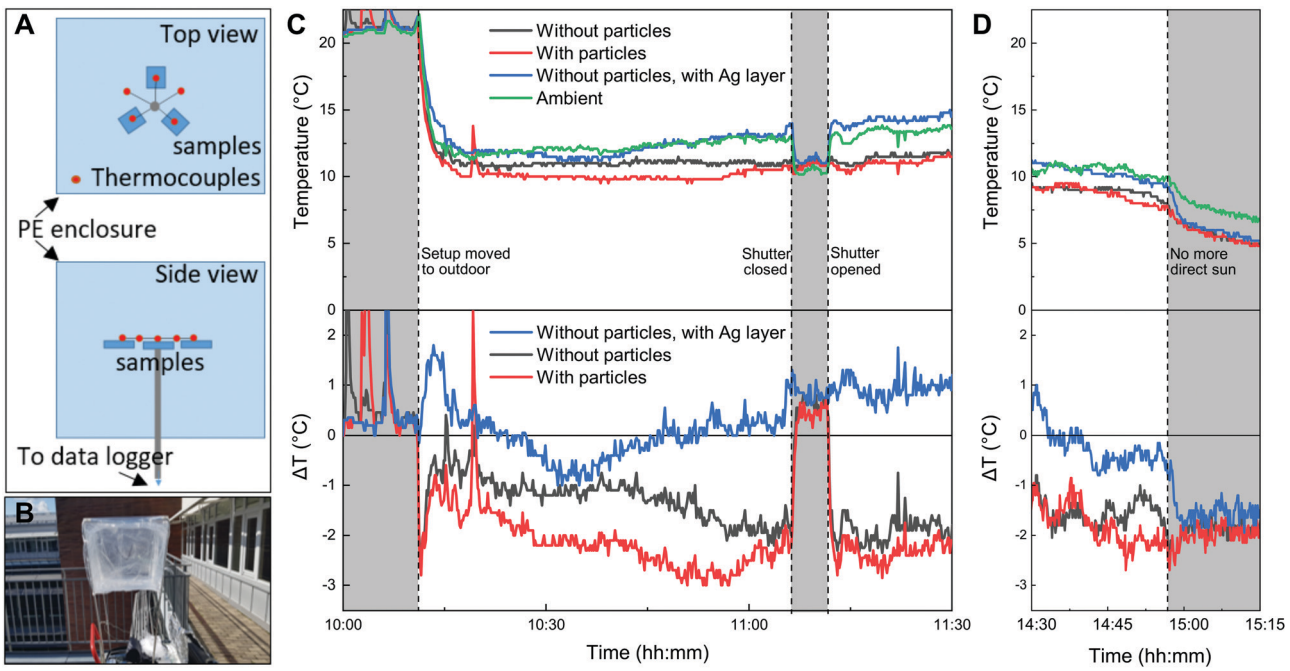

Fig. 5 Radiative cooling performance. Temperature measurements of samples with and without microparticles and an additional sample with Ag bottom layer and no microparticles. (A) Schematics of the temperature measurement apparatus. (B) Image of the real-time temperature measurement setup. (C and D) Temperature and ΔT (= $T_{sample} - T_{ambient}$) values of the three samples at two different time windows during measurements. The line colors in (D) are the same as in (C).

setup was taken outdoor (at about 10:10 am). The temperature spike for the sample with particles at around 10:20 (red line in Fig. 5C) is due to a thermal disturbance caused while manually adjusting the sample position. More interestingly, both the samples with and without microparticles quickly reached temperatures lower than the ambient temperature. This result suggests that the samples effectively released heat to the sky by passive radiative cooling. The metamaterial sample with microparticles showed the largest decrease in temperature, as also evident from ΔT in Fig. 5C. Our observed subambient temperature decrease of around 2–3 °C is on the same order as for previous works on daylight radiative cooling during mid-day. For example, Gentle and Smith[53] presented around 2 °C subambient cooling for a material based on a Vikuiti enhanced specular reflector film; Mandal *et al.*[54] reported around 6 °C for a hierarchically porous poly(vinylidene fluoride-*co*-hexafluoropropene) material; Li *et al.*[24] achieved around 5 °C cooling during mid-day for delignified wood, and up to around 10 °C cooling at other times during their measurement. In contrast to the two transparent samples, the paper with reflective Ag back coating did not clearly lower its temperature relative to the surroundings. We attribute this result to non-negligible solar absorption by the silver layer deposited on the relatively rough paper surface (it also looked yellowish to the naked eye, see Fig. S4, ESI†). This hypothesis is further supported by the decrease in temperature of the Ag-coated sample when no longer being exposed by direct sun light but still exposed to the clear sky (just before 15.00, see Fig. 5D). For such conditions, the Ag coated sample showed clear passive radiative cooling just as the transparent samples. The results highlight the need for optimizing reflective coatings in terms of smoothness and quality to achieve ideal reflection with minimal absorption. Nonetheless, we have obtained clear daytime cooling of up to 4 °C also for another Ag coated sample, as shown in Fig. S5 (ESI†). To further investigate the effect of exposure to the sun under a clear sky, we covered the setup with a metal foil for a few minutes (between 11:00 and 11:15 in Fig. 5C). As expected, the covered samples lost their ability to maintain a lower temperature than the surrounding, in agreement with no longer being able to perform effective passive radiative cooling. The higher ambient temperature in the PE enclosure when exposed to solar irradiation could be explained by some solar absorption inside the enclosure. Indeed, the temperature in the enclosure was typically a few degrees higher than the outside atmospheric temperature in sunny conditions.

4. Conclusion

We have reported a metamaterial nanocellulose–microparticle composite with controllable translucency, minimal visible absorption, and strong IR absorption. To our knowledge, this is the first study that integrates tunable translucency in the visible range with high IR absorption for a composite material, and the first study exploring radiative cooling based on a nanocellulose composite. In the visible range, the microparticles act as non-absorbing scatterers and the concentration of microparticles in the paper controls the translucency from essentially no haze for papers without microparticles, to 90% haze for papers with 10.3 wt% of microparticles with 1.18 μm diameter. The IR absorption remained high for both samples with and without microparticles, with only small variations due to the different absorption properties of the constituents. Hence, the visible translucent diffusion could be varied from 0 to 90% without having any significant change in the IR absorption characteristics. Moreover, the visible absorption remained minimal for all compositions of the paper. The high emissivity in the atmospheric IR window range combined with low visible absorption make the composites suitable for passive radiative cooling, even in sunny conditions during daytime. We demonstrated this capability *via* passive radiative cooling experiments, which show several degrees Celsius decrease in temperature relative to the surrounding environment. The combination of high haze, low visible absorption and high thermal emissivity makes the nanocellulose metamaterials interesting for use as coatings in optoelectronic devices such as solar cells, for which the combined set of properties may enhance device light absorption while also improving life time by passive radiative cooling.

Conflicts of interest

The authors declare no conflicts of interest.

Acknowledgements

The authors acknowledge financial support from the Knut and Allice Wallenberg Foundation *via* a Wallenberg Scholarship; the Knut and Alice Wallenberg foundation, Linköping University and industry through the Wallenberg Wood Science Center; the Swedish Government Strategic Research Area in Materials Science on Functional Materials at Linköping University (Faculty Grant SFO-Mat-LiU No. 2009 00971), the Swedish Foundation for Strategic Research and the Swedish Armed Forces Research and Technology programme. The authors also thank Meysam Karami Rad for help with constructing the temperature and cooling power measurement setup.

References

1 A. Baptista, I. Ferreira and J. Borges, Cellulose-Based Bioelectronic Devices, *Cellulose – Medical, Pharmaceutical and Electronic Applications*, 2013, DOI: 10.5772/56721.
2 T. G. M. Van De Ven, *Cellulose – Medical, Pharmaceutical and Electronic Applications*, IntechOpen, London, 2013.
3 S. M. Mahpeykar, *et al.*, Cellulose Nanocrystal:Polymer Hybrid Optical Diffusers for Index-Matching-Free Light Management in Optoelectronic Devices, *Adv. Opt. Mater.*, 2017, **5**(21), 1700430, DOI: 10.1002/adom.201700430.
4 W. Wu, N. G. Tassi, H. L. Zhu, Z. Q. Fang and L. B. Hu, Nanocellulose-based Translucent Diffuser for Optoelectronic Device Applications with Dramatic Improvement of Light Coupling, *ACS Appl. Mater. Interfaces*, 2015, **7**, 26860–26864.
5 A. Espinha, *et al.*, Hydroxypropyl cellulose photonic architectures by soft nanoimprinting lithography, *Nat. Photonics*, 2018, **12**, 343–348, DOI: 10.1038/s41566-018-0152-1.

6 A. G. Dumanli, *et al.*, Controlled, bio-inspired self-assembly of cellulose-based chiral reflectors, *Adv. Opt. Mater.*, 2014, **2**(7), 646–650, DOI: 10.1002/adom.201400112.
7 S. N. Fernandes, *et al.*, Mind the Microgap in Iridescent Cellulose Nanocrystal Films, *Adv. Mater.*, 2017, **29**(2), 1603560, DOI: 10.1002/adma.201603560.
8 H. Águas, *et al.*, Thin Film Silicon Photovoltaic Cells on Paper for Flexible Indoor Applications, *Adv. Funct. Mater.*, 2015, **25**(23), 3592–3598, DOI: 10.1002/adfm.201500636.
9 D. Ha, Z. Fang, L. Hu and J. N. Munday, Paper-based anti-reflection coatings for photovoltaics, *Adv. Energy Mater.*, 2014, **4**(9), 1301804, DOI: 10.1002/aenm.201301804.
10 A. Espinha, *et al.*, Shape memory cellulose-based photonic reflectors, *ACS Appl. Mater. Interfaces*, 2016, **8**(46), 31935–31940, DOI: 10.1021/acsami.6b10611.
11 T. Wu, *et al.*, A bio-inspired cellulose nanocrystal-based nanocomposite photonic film with hyper-reflection and humidity-responsive actuator properties, *J. Mater. Chem. C*, 2016, **4**, 9687–9696, DOI: 10.1039/c6tc02629j.
12 Z. Fang, *et al.*, Novel nanostructured paper with ultrahigh transparency and ultrahigh haze for solar cells, *Nano Lett.*, 2014, **14**(2), 765–773, DOI: 10.1021/nl404101p.
13 H. Zhu, *et al.*, Transparent nanopaper with tailored optical properties, *Nanoscale*, 2013, **5**, 3787–3792, DOI: 10.1039/c3nr00520h.
14 H. Y. Yu, G. Y. Chen, Y. B. Wang and J. M. Yao, A facile one-pot route for preparing cellulose nanocrystal/zinc oxide nanohybrids with high antibacterial and photocatalytic activity, *Cellulose*, 2015, **22**, 261–273.
15 H. P. Kuo, M. Y. Chuang and C. C. Lin, Design correlations for the optical performance of the particle-diffusing bottom diffusers in the LCD backlight unit, *Powder Technol.*, 2009, **192**(1), 116–121, DOI: 10.1016/j.powtec.2008.12.003.
16 M. Liu, D. Wu, Y. Zhang and J. Zhuang, Optimization and design of LCD diffuser plate with micro-semisphere structure, *Procedia Eng.*, 2011, **16**, 306–311, DOI: 10.1016/j.proeng.2011.08.1088.
17 M. L. Brongersma, Y. Cui and S. Fan, Light management for photovoltaics using high-index nanostructures, *Nat. Mater.*, 2014, **13**, 451–460, DOI: 10.1038/nmat3921.
18 B. Wu and Q. K. Wang, High sensitivity transmission-type SPR sensor by using metallic-dielectric mixed gratings, *Chin. Phys. Lett.*, 2008, **25**(5), 1668–1671, DOI: 10.1088/0256-307X/25/5/040.
19 C. Y. Chen, *et al.*, Enhancing Optical Out-Coupling of Organic Light-Emitting Devices with Nanostructured Composite Electrodes Consisting of Indium Tin Oxide Nanomesh and Conducting Polymer, *Adv. Mater.*, 2015, **27**(33), 4883–4888, DOI: 10.1002/adma.201502516.
20 L. Zhou, *et al.*, Multiscale micro-nano nested structures: Engineered surface morphology for efficient light escaping in organic light-emitting diodes, *ACS Appl. Mater. Interfaces*, 2015, 7(48), 26989–26998, DOI: 10.1021/acsami.5b08575.
21 X. Zhang, Y. Huang, X. Ren, H. Huang and Q. Wang, Flat-top steep-edge photodetector with cascaded grating structure, *Appl. Opt.*, 2009, **48**(35), 6760–6764, DOI: 10.1364/AO.48.006760.
22 M. A. Tshabalala, Surface characterization, in *Handbook of wood chemistry and wood composites*, ed. R. M. Rowell, CRS Press, 2013, pp. 196–198.
23 M. Rahimi Kord Sofla, R. J. Brown, T. Tsuzuki and T. J. Rainey, A comparison of cellulose nanocrystals and cellulose nanofibres extracted from bagasse using acid and ball milling methods, *Adv. Nat. Sci.: Nanosci. Nanotechnol.*, 2016, **7**(3), 035004, DOI: 10.1088/2043-6262/7/3/035004.
24 T. Li, *et al.*, A radiative cooling structural material, *Science*, 2019, **364**(6442), 760–763, DOI: 10.1126/science.aau9101.
25 S. Y. Lin, *et al.*, Enhancement and suppression of thermal emission by a three-dimensional photonic crystal, *Phys. Rev. B: Condens. Matter Mater. Phys.*, 2000, **62**(4), R2243–R2246, DOI: 10.1103/PhysRevB.62.R2243.
26 A. Narayanaswamy and G. Chen, Thermal emission control with one-dimensional metallodielectric photonic crystals, *Phys. Rev. B: Condens. Matter Mater. Phys.*, 2004, **70**(12), 125101, DOI: 10.1103/PhysRevB.70.125101.
27 J. A. Schuller, T. Taubner and M. L. Brongersma, Optical antenna thermal emitters, *Nat. Photonics*, 2009, **3**, 658–661, DOI: 10.1038/nphoton.2009.188.
28 A. Lenert, *et al.*, A nanophotonic solar thermophotovoltaic device, *Nat. Nanotechnol.*, 2014, **9**, 126–130, DOI: 10.1038/nnano.2013.286.
29 A. P. Raman, M. A. Anoma, L. Zhu, E. Rephaeli and S. Fan, Passive radiative cooling below ambient air temperature under direct sunlight, *Nature*, 2014, **515**, 540–544.
30 Y. Zhai, *et al.*, Scalable-manufactured randomized glass-polymer hybrid metamaterial for daytime radiative cooling, *Science*, 2017, **355**(6329), 1062–1066, DOI: 10.1126/science.aai7899.
31 L. Zhou, *et al.*, A polydimethylsiloxane-coated metal structure for all-day radiative cooling, *Nat. Sustainable*, 2019, **2**, 718–724, DOI: 10.1038/s41893-019-0348-5.
32 J. Mandal, *et al.*, Hierarchically porous polymer coatings for highly efficient passive daytime radiative cooling, *Science*, 2018, **362**, 315–319.
33 S. Catalanotti, *et al.*, The radiative cooling of selective surfaces, *Sol. Energy*, 1975, **17**, 83–89.
34 B. Bartoli, *et al.*, Nocturnal and diurnal performances of selective radiators, *Appl. Energy*, 1977, **3**(4), 267–286, DOI: 10.1016/0306-2619(77)90015-0.
35 Y. Huang, *et al.*, Ultra-broadband large-scale infrared perfect absorber with optical transparency, *Appl. Phys. Express*, 2017, **10**(11), 112601, DOI: 10.7567/APEX.10.112601.
36 X. Lu, P. Xu, H. Wang, T. Yang and J. Hou, Cooling potential and applications prospects of passive radiative cooling in buildings: the current state-of-the-art, *Renewable Sustainable Energy Rev.*, 2016, **65**, 1079–1097, DOI: 10.1016/j.rser.2016.07.058.
37 N. M. Nahar, P. Sharma and M. M. Purohit, Performance of different passive techniques for cooling of buildings in arid regions, *Build. Environ.*, 2003, **38**(1), 109–116, DOI: 10.1016/S0360-1323(02)00029-X.
38 L. Zhu, A. P. Raman and S. Fan, Radiative cooling of solar absorbers using a visibly transparent photonic crystal

thermal blackbody, *Proc. Natl. Acad. Sci. U. S. A.*, 2015, **112**(40), 12282–12287, DOI: 10.1073/pnas.1509453112.

39 W. Li, Y. Shi, K. Chen, L. Zhu and S. Fan, A Comprehensive Photonic Approach for Solar Cell Cooling, *ACS Photonics*, 2017, **4**(4), 774–782, DOI: 10.1021/acsphotonics.7b00089.

40 A. W. Harrison, Effect of atmospheric humidity on radiation cooling, *Sol. Energy*, 1981, **26**(3), 243–247, DOI: 10.1016/0038-092X(81)90209-7.

41 M. Dong, N. Chen, X. Zhao, S. Fan and Z. Chen, Nighttime radiative cooling in hot and humid climates, *Opt. Express*, 2019, **27**(22), 31587–31598, DOI: 10.1364/oe.27.031587.

42 T. Suichi, A. Ishikawa, Y. Hayashi and K. Tsuruta, Performance limit of daytime radiative cooling in warm humid environment, *AIP Adv.*, 2018, **8**(5), 055124, DOI: 10.1063/1.5030156.

43 C. Sheng, Y. An, J. Du and X. Li, Colored Radiative Cooler under Optical Tamm Resonance, *ACS Photonics*, 2019, **6**(10), 2545–2552, DOI: 10.1021/acsphotonics.9b01005.

44 Y. Chen, *et al.*, Colored and paintable bilayer coatings with high solar-infrared reflectance for efficient cooling, *Sci. Adv.*, 2020, **6**(17), eaaz5413, DOI: 10.1126/sciadv.aaz5413.

45 L. Zhu, A. Raman, K. X. Wang, M. A. Anoma and S. Fan, Radiative cooling of solar cells, *Optica*, 2014, **1**(1), 32–38, DOI: 10.1364/optica.1.000032.

46 D. Zhao, *et al.*, Radiative sky cooling: Fundamental principles, materials, and applications, *Appl. Phys. Rev.*, 2019, **6**(2), 021306, DOI: 10.1063/1.5087281.

47 L. Hu, *et al.*, Transparent and conductive paper from nanocellulose fibers, *Energy Environ. Sci.*, 2013, **6**(2), 513–518, DOI: 10.1039/c2ee23635d.

48 C. F. Bohren and D. R. Huffman, Surface modes in small particles, *Absorption and Scattering of Light by Small Particles*, WILEY-VCH Verlag GmbH & Co., 1998, pp. 325–331.

49 B. Miller, *et al.*, Tuning the Fröhlich exciton-phonon scattering in monolayer MoS_2, *Nat. Commun.*, 2019, **10**, 807, DOI: 10.1038/s41467-019-08764-3.

50 X. Sun, Y. Sun, Z. Zhou, M. A. Alam and P. Bermel, Radiative sky cooling: fundamental physics, materials, structures, and applications, *Nanophotonics*, 2017, **6**(5), 997–1015, DOI: 10.1515/nanoph-2017-0020.

51 J.-J. Greffet, P. Bouchon, G. Brucoli, E. Sakat and F. Marquier, Light Emission by Nonequilibrium Bodies: Local Kirchhoff Law, *Phys. Rev. X*, 2016, **8**, 021008, DOI: 10.1103/PhysRevX.8.021008.

52 M. Kranjčec, I. P. Studenyak and M. V. Kurik, Urbach rule and disordering processes in Cu6P(S 1-xSex)5Br1-yIy superionic conductors, *J. Phys. Chem. Solids*, 2006, **67**(4), 807–817, DOI: 10.1016/j.jpcs.2005.10.184.

53 A. R. Gentle and G. B. Smith, A Subambient Open Roof Surface under the Mid-Summer Sun, *Adv. Sci.*, 2015, **2**(9), 1500119, DOI: 10.1002/advs.201500119.

54 J. Mandal, *et al.*, Hierarchically porous polymer coatings for highly efficient passive daytime radiative cooling, *Science*, 2018, **362**(6412), 315–319, DOI: 10.1126/science.aat9513.

